Astron. Astrophys. 206, 136–142 (1988)

ASTRONOMY
AND
ASTROPHYSICS

The anomalous dust tail of comet Kohoutek (1973 XII) near perihelion

K. Richter and H. U. Keller

Max-Planck-Institut für Aeronomie, D-3411 Katlenburg-Lindau, Federal Republic of Germany

Received May 9, accepted June 27, 1988

Summary. The anomalous tail of comet Kohoutek (1973 XII) observed by the White Light Coronagraph on board Skylab at the end of December 1973 is interpreted based on a recently developed model. The unique observations show an extended anomalous dust tail of more than 2 Gm in length pointing apparently towards the sun. The appearance of the tail changed dramatically within days. For two days it looked like a sharp spike. Brightness profiles across this spike have been calculated for a variety of dust grain size distributions and dust production rates using the method of Richter and Keller (1987). Finite emission velocities and Keplerian trajectories of the dust particles are used instead of approximations. It is shown that the effect of focussing of the dust particles along their nodal lines is important for the formation of the observed sharp spike and its variation with time. Previous investigations have suggested a major excess of large particles. This is not supported by the present investigation. All earlier efforts have been based on the Finson and Probstein approach for zero emission velocities of the dust particles and therefore could not include the effect of focussing. A satisfactory interpretation of the observations is found for a dust production rate proportional to r^{-2} and mass distribution $h(m) \propto m^{-1.8}$ where r is the heliocentric distance.

Key Words: cometary dust – nodal line – cometary tail

1. Introduction

Cometary dust particles are dragged away from the comet by subliming gas molecules. After a very short interaction region in the range of a kilometre or less, the particles reach their terminal ejection velocities. The corresponding hydrodynamic dust acceleration processes have been studied by several authors (e.g. Probstein, 1968; Hellmich, 1981; Gombosi et al., 1985). Thereafter, the Keplerian motions of the particles are controlled by solar gravity and radiation pressure force. Mechanical theories based on the assumption of "reduced" solar gravity have been developed already by Bessel (1836) and Bredikhin (around 1900). The appearance of a dust tail is determined by the dust production rate and its variation with time, the orbit of the comet, the emission velocities of the particles, and their acceleration controlled by the ratio of radiation pressure force to gravitational attraction. This ratio depends on the particle composition (scattering properties), size, and density. The dust particles are always pushed in the antisolar direction relative to the nucleus and the dust tails form in the antisolar direction. Under certain geometric conditions a tail can appear pointing sunward as a result of its projection onto the sky plane (Sekanina, 1974a).Comet Kohoutek (1973 XII) showed an anomalous tail from the end of December 1973 for several months. Model calculations for the anomalous tail of comet Kohoutek have been carried out by Sekanina (1974b) using the Finson and Probstein (1968) approach for zero emission velocity. Calculations by Keller et al. (1983) have shown, that this approach can only very crudely explain the appearance of the observed spike in December 1973 and does not explain its variation with time. Qualitative considerations support the assumption that focussing of dust particles in the orbital plane of the comet plays a role. This focussing occurs at true anomalies that correspond to the nodal lines of the respective emission dates. Since the more general Finson and Probstein approach for finite emission velocities is based on the assumption of expanding hypothetical spherical shells of dust particles with finite ejection velocities around a particle with zero velocity it cannot reproduce the focussing. We have developed a novel model to calculate the dust density of cometary tails rigorously (Richter and Keller, 1987). Keplerian trajectories are used rather than approximations. In this paper we present photographs of the sharp spike of comet Kohoutek and the results of appropriate calculations to explain its appearance (column density) and its variation with time.

Send offprint requests to: K. Richter

2. Observations

Approximately 1600 photographs of comet Kohoutek were obtained through the High Altitude Observatory's White Light Coronagraph on Skylab around the time of perihelion passage at the end of December 1973 (MacQueen et al., 1974). The resolution of the images taken by the space born coronagraph is only about 10′. The signal to noise ratio is limited by the high background of the solar corona for images centred on the sun and by scattered light when the instrument was "misused" pointing off the sun. The four best and also characteristic photographs with the frame numbers 28455, 29318, 29446, 29760 are presented and investigated. The corresponding positions of the earth and the comet in a heliocentric coordinate system are illustrated in Fig. 1. The lines of sight are close to the orbital plane of the comet, the elevation angle of the earth above the cometary orbital plane varies from 3°.78 to 4°.75. In Fig. 2 the vectors represent projections of the heliocentric velocity of the comet onto the sky plane as seen from the earth. The sunward directed dashed lines indicate

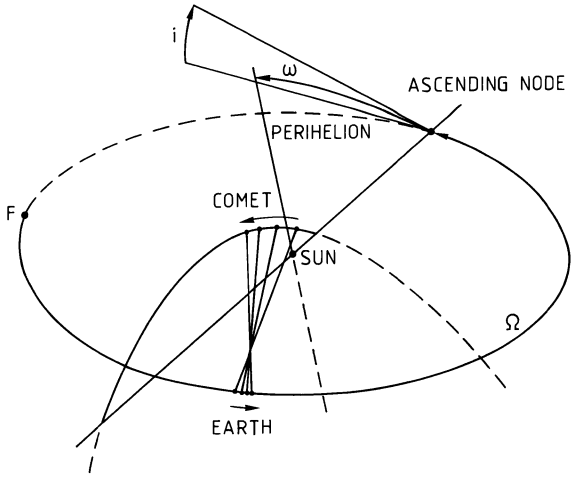

Fig. 1. The orbit of comet Kohoutek (1973 XII) in a heliocentric coordinate system. Its position for the frames 28455 to 29760 are shown connected by lines with the earth. $T = 1973$ Dec. 28.43067, $i = 14°.2969$, $\Omega = 257°.7656$, $\omega = 37°.8238$, $e = 1.0000078$, $q = 0.1424249$ (1950) are used for the ephemerides

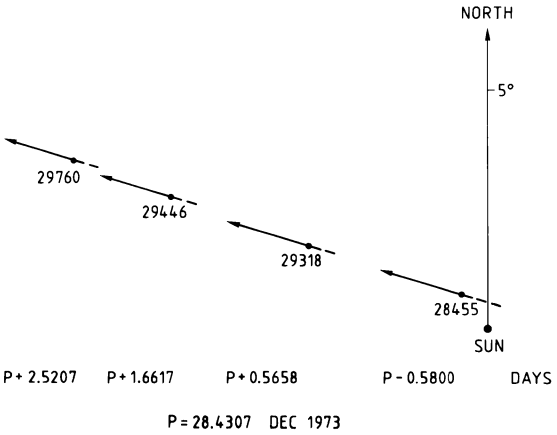

Fig. 2. The positions of comet Kohoutek (1973 XII) in the sky plane for the frames 28455 to 29760. The vectors represent the projected heliocentric velocities of the comet

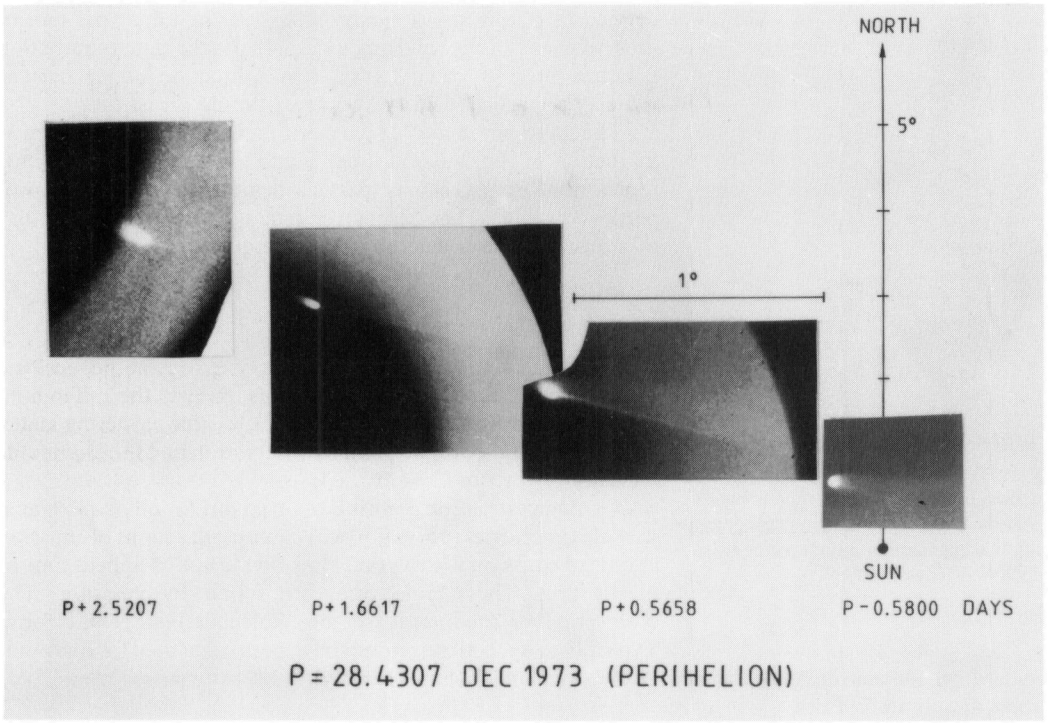

Fig. 3. Photomontage of frames 28455 to 29760 in the sky plane. The photographs are enlarged by a factor 3 with respect to the right hand scale

therefore the limits for the synchrones and syndynes for old and large particles. The orientations and the scales of the photographs have been checked and improved using stars identified on the photographs. As expected the spike of the anomalous tail is oriented close to the projected orbital velocity. Figure 3 is a sequence of the four photographs and is arranged in the same way as Fig. 2. Note that the photographs are enlarged by a factor 3 with respect to the scale on the right hand side. The details of Fig. 3 are summarized in Table 1.

The photograph 28455 was taken about half a day before the comet passed through perihelion. The coronagraph was pointed directly at the sun. The anomalous tail looked like a fan at that time, however, a concentration of material towards the southern boundary of the fan is apparent. About one day later (photograph 29318) an extended, marked spike with a length of about 60′ and a width of 0.′7 was the most prominent feature of the comet. The fan like structure of the anomalous tail was faintly visible northward of the spike. For this and the following photographs, the optical

Table 1

Frame	28455	29318	29446	29760
Time of Observation (UT) (day of Dec. 1973)	27.8507	28.9965	30.0924	30.9514
Time to Perihelion (days)	-0.5800	0.5658	1.6617	2.5207
Elongation angle Sun-Earth-Comet	0.°915	4.°21	7.°28	9.°47
Position angle of the Sun	216.°0	245.°0	247.°2	247.°6
Angle between the radial direction from the Sun and the velocity vector (calculated)	38.°48	8.°84	6.°29	5.°78
Measured angle between direction towards the Sun and the spike	40.°0 ± 2°	8.°5 ± 1°	6.°2 ± 1°	12.°5 ± 2°
Elevation angle of the Earth above the cometary orbital plane	3.°78	4.°10	4.°45	4.°75
Scattering angle Sun-Comet-Earth	6.°18 173.°82	29.°93 150.°07	50.°75 129.°25	63.°2 116.°8
Approx. visible length of the spike	15'	60'	60'	7'

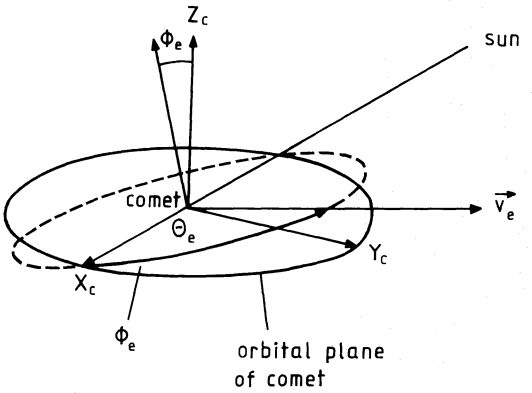

Fig. 4. The emission velocity v_e of a dust particle in the moving cometary system. The x_c coordinate of the righthanded Cartesian coordinate system points away from the sun, z_c is parallel to the orbital angular momentum vector of the comet. v_e, θ, φ are the spherical coordinates of v_e with respect to y_c, z_c, x_c

axis of the coronagraph was pointed off the sun direction. The level of scattered light was strong in this unforeseen mode of operation. On the next photograph 29466 the distinct spike had nearly the same length but its width appeared to be narrower ($\approx 0.'4$). The visible length of the spike was less than 10' on the last photograph (29760). The fast variations of the appearance of the anomalous tail are remarkable but explained by the fast changes of the observational geometry. The angular velocity of the comet near its close perihelion (0.14 AU) is large (26°/day).

The photographs were scanned by a microdensitometer with a linear resolution of 24″ for frame 28455 and 9.″6 for the other frames. A running window was applied with a box size of 0.′2 across an 2' along the spike in order to reduce the noise of the data.

Three components contributed to the total brightness recorded by the coronagraph

$$B_{\text{tot}} = B_{\text{scat}} + T \cdot (B_{\text{obj}} + B_{\text{back}}),$$

where B_{scat} was the scattered or stray light introduced by the instrument, T was the transmission (including vignetting), B_{obj}, B_{back} were the brightness of the object and the background (mainly F-corona), respectively.

Since the stray light strongly increased when the coronagraph was pointed away from the sun, only rough absolute brightness evaluations of the spike could be obtained especially for frames 29446 and 29760. The results are presented and discussed in Sect. 5.

3. The method for the brightness calculations

Here, the basic relations used for the calculations are only briefly summarized. A detailed description of the method was published by Richter and Keller (1987).

The brightness B for a point in the sky plane (single scattering) can be described by the integral over all points along the line of sight, L

$$B = \int_L \int_{\tau_1}^{\tau_2} N(\tau, \beta, \theta, \varphi) \frac{\sin\theta}{|J|} \sigma(\alpha) \frac{I}{r_s^2} \, d\tau \, dl. \quad (1)$$

$N(\tau, \beta, \theta, \varphi)$ is the number of particles emitted in the direction defined by θ, φ in the cometary system at the time τ per unit of time, of β, and of the solid angle (Fig. 4). β is the ratio of radiation pressure force to gravity force, it is a function of the particle radius, the particle density and its scattering properties.

The speed of the emitted particles, v_e, is assumed to be given as a function of the emission time, τ, and the particle size which is represented by β (keeping particle density and scattering properties constant). Then, for a given time τ the Keplerian trajectory of a dust particle is determined by the quantities β, θ, φ and

$$J = \frac{\partial(x, y, z)}{\partial(\beta, \theta, \varphi)}$$

is the Jacobian determinant, where x, y, z are the heliocentric coordinates of the trajectory endpoints. $\sigma(\alpha)$ is the differential scattering cross section ($\text{cm}^2 \cdot \text{sterad}^{-1}$), α is the scattering angle, r_s the solar distance to the point of observation and I the luminous intensity of the sun ($2.84\ 10^{27}$ cd).

The integration for B must be carried out for all possible dust particle trajectories (normally two) connecting a point of emission at time of emission with a point lying on the line of sight at time of observation. These trajectories are found by iteration. The corresponding Jacobians are then calculated in closed form. Typically about 600 trajectories have been calculated for one point in the sky plane (column density).

4. The dust model

The dependence of the brightness profiles (perpendicular to the spike direction) on several parameters have been investigated. The calculations are numerically demanding and, therefore, the parameter ranges have to be judicially restricted. Simple expressions for N and v_e have therefore been used. The following relations are considered

- the total dust production rate is proportional to $r^{-z}(\tau)$,
- the particle mass distribution varies according to $h(m) \propto m^{-s}$,
- the dust outflow only depends on the angle θ in the cometary system. For simplicity the outflow is assumed to be uniform within a cone with a full opening angle of $2\theta_0$ centred on the comet-sun line at time of emission,

– the emission velocities are assumed to be constant within the emission cone and the relation

$$v_e(r_s) = \frac{v_0}{r_s}\sqrt{\beta}\,[\mathrm{km\,s^{-1}}], \tag{2}$$

describes the change of v_e with heliocentric distance, r_s[AU].

In the literature, the particle size distribution $g(a)$ is often used instead of $h(m)$. $g(a) \propto a^{-(3s-2)}$ corresponds to $h(m) \propto m^{-s}$.

v_e is assumed to be independent of z, s, θ_0 although the dust size distribution and the ratio of gas to dust production are also parameters which govern the process of hydrodynamic dust acceleration. The solutions for the trajectories depend only on v_e. A typical number of trajectories used for one profile is 20,000.

The proportionality of v_e to $\sqrt{\beta}$ is a rather good approximation, especially for large particles. The outflow velocity is influenced by the surface temperature and the gas (dust) emission rate of the comet as a function of heliocentric distance. This is approximated by introducing a $1/r_s$ dependence. $v_0 = 1\,\mathrm{km\,s^{-1}}$ yields emission velocities compatible with model calculations for comet Halley (Divine et al., 1986).

τ is limited to $\leqq 300$ days, $\beta \leqq 1$, and $v_0/r_s \leqq 2$ to avoid cumbersome complications in finding the dust particle trajectories for extreme and irrelevant parameter values. These limits do not seriously affect the results.

For a given type of spherical dust particle it holds

$$\beta = 0.6\ 10^{-3}\,\frac{Q_{\mathrm{pr}}}{\varrho a}, \tag{3}$$

where a is its radius in [m], ϱ its density in [$\mathrm{kg\,m^{-3}}$] and Q_{pr} is the scattering efficiency for radiation pressure (Van de Hulst, 1957). Then, N can be expressed by

$$N \propto r^{-z}(\tau)\,\beta^{3s-4}\,f(\theta) \tag{4}$$

with

$$f(\theta) = \begin{cases} \dfrac{2}{1-\cos\theta_0}, & \pi-\theta \leqq \theta_0 \\ 0, & \pi-\theta > \theta_0. \end{cases}$$

The differential scattering cross section $\sigma(\alpha)$ for spherical particles can be written as

$$\sigma(\alpha) = A_p a^2\,\chi(\alpha), \tag{5}$$

where A_p is the geometric albedo and χ its angle dependent part normalized so that $\chi(180°) = 1$. For large particles ($a \gg \lambda$) we assume $A_p = \mathrm{const}$ then

$$\sigma(\alpha) \propto \beta^{-2}\,\chi(\alpha). \tag{6}$$

α varies from 174° to 117°, see Table 1.

5. Results

Brightness profiles across the spike at increasing distances from the nucleus have been calculated for various values of the parameters s, z, v_0, θ_0. Figures 5 and 6 illustrate the influence of these parameters on the brightness profiles at an angular distance of 16′ from the nucleus for photograph 29446. The surface brightness is given in arbitrary units. Different scaling factors are used for different parameters s and z. The x-axis is counted from the negative velocity vector of the comet projected onto the sky plane in units of arcminutes, positive values being northward (see Fig. 2).

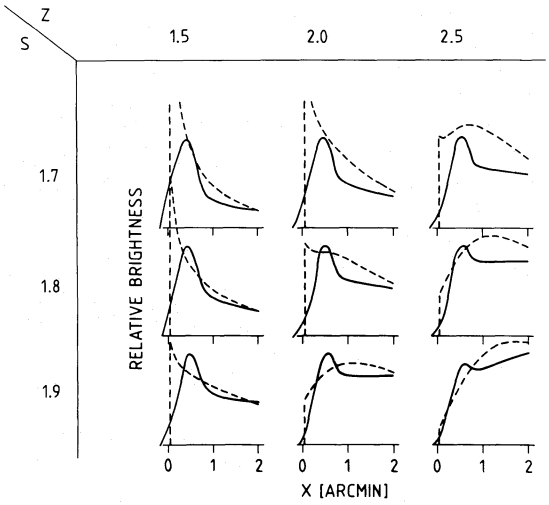

Fig. 5. Calculated relative brightness (linear scale) across the spike of comet Kohoutek for a matrix of the parameters s and z. The distance of the cross scan from the centre of brightness (nucleus) is 16′. The dashed lines correspond to the Finson and Probstein approach with zero emission velocity

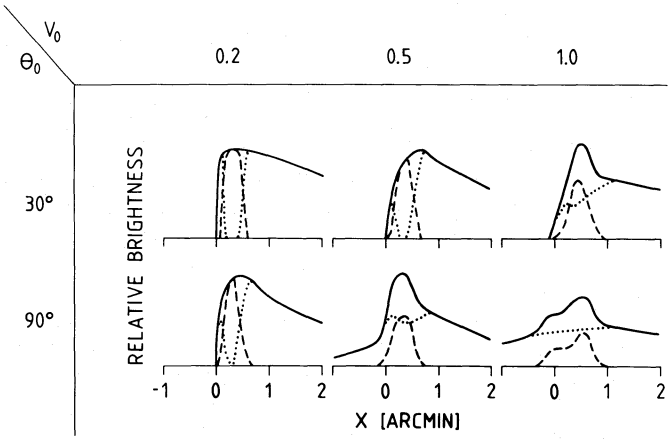

Fig. 6. Calculated relative brightness (linear scale) across the spike of comet Kohoutek for a matrix of the parameters θ_0, v_0, see caption of Fig. 5 for more details

Figure 5 shows a matrix of profiles for $s = 1.7$, 1.8, 1.9 and $z = 1.5$, 2.0, 2.5. In this example $v_0 = 1.0$, $\theta_0 = 30°$. The results of a computation using the Finson and Probstein approach with zero emission velocity are overlayed as dashed lines for comparison. Earlier investigations using this approach have shown, that old and large particles are concentrated near the comet's trajectory, whereas younger and smaller particles are located northward on the sky plane. Therefore small values of s and z e.g. $s \lesssim 1.8$ and $z \lesssim 2$ support the appearance of a spike and vice versa (Sekanina, 1974; Keller et al. 1983). Complementary sets of s and z can yield similar profiles. That means increasing z values can roughly be compensated by decreasing s values.

However, a hump is still visible for those s, z values for which the zero emission velocity profiles do not allow the appearance of a spike. This important result is caused by the focussing of dust particles around their nodal lines. Figure 6 shows brightness profiles for $v_0 = 0.2$, 0.5, 1.0 and $\theta_0 = 30°$, 90° while $s = 1.8$ and $z = 2.0$. The total brightness contribution (full lines) is split into two components stemming from two different geometric con-

ditions between the point of emission P_e and the point of observation P_0. The dust particles can be characterized by the true anomaly of their trajectories given by the angle $\psi = P_e S P_0$ where S corresponds to the sun. The dashed lines depict contributions from particles with $|\psi - 180°| \leqq 10°$. Particles for which $\psi = 180°$ are just recrossing the orbital plane of the comet at observation time independent of their emission velocity. The dotted curves belong to $|\psi - 180°| > 10°$. For $v_0 = 0.2\,\mathrm{km\,s^{-1}}$ and $\theta_0 = 30°$ the overlapping of the two contributions can be neglected and the brightness profile is similar to the zero emission velocity approach ($v_0 = 0$). With increasing values of v_0, θ_0 the dotted profiles become smoother and fill up the minimum, whereas the dashed curves remain narrow because the corresponding particles are contracted closer to the orbital plane of the comet. Therefore, a hump appears.

We point out, that $v_0 = 0.5\,\mathrm{km\,s^{-1}}$ and $\theta_0 = 90°$ one side and $v_0 = 1.0$, $\theta_0 = 30°$ on the other side yield simhlar profiles. This is also the case for $v_0 = 0.2\,\mathrm{km\,s^{-1}}$, $\theta_0 = 90°$ and $v_0 = 0.5\,\mathrm{km\,s^{-1}}$, $\theta_0 = 30°$, respectively. This is plausible. Since the earth was close to the orbital plane of the comet at that time, the deviation from the brightness profiles based on the zero emission velocity model was mainly caused by dust particles emitted perpendicularly to that plane. That means v_0, θ_0 can be combined into one parameter $v_0 \sin\theta_0$ for approximate calculations.

The task to determine a unique set of the parameters z, s, v_0, θ_0, e.g., by a least square fit to the observations is not feasible for at least two reasons. The large number of dust particle trajectories which must be found by iteraton for even one value of v_0 requires a prohibitive amount of CPU time. The influence of the parameters on the solution is in many cases compensatory and different sets s, z, v_0, θ_0 yield similar profiles. Variations of z can be compensated by variations of s; a similar relationship is found between v_0, θ_0 (see above). Therefore z, v_0 have been fixed and s, θ_0 have been varied. Unique solutions may not exist.

Infrared observations of comet Kohoutek have shown that the mass loss rate can be approximated by $M \propto r^{-2}$ within 1 AU (Ney, 1982). As mentioned above $v_0 = 1\,\mathrm{km\,s^{-1}}$ could be considered a realistic value. For $z = 2$ and $v_0 = 1\,\mathrm{km\,s^{-1}}$ and various values for s and θ_0 brightness profiles at the distances 8′, 16′, and 40′ from the nucleus have been calculated and compared with the observations. First we present the results, later we will give an overview of the dependence of the profiles on these parameters. Figure 7 shows the calculated profiles for $s = 1.8$ and $\theta_0 = 30°$. The brightness of the profiles is given in arbitrary units in a logarithmic scale. The profiles for zero emission velocity are drawn in as dashed curves for comparison. The right hand cut offs for frames 28455 and 29318 correspond to the cut off for particles with $\beta > 1$. The dotted curves for frames 29446 and 29760 are the contributions from dust particles with $|\psi - 180°| > 10°$. For this figure $\chi(\alpha) = 1$ was chosen.

The profiles show the development of the sharp spike and its fading as well as the fan like structure especially for frame 28455 and 29318 in good agreement with the observations. ψ is $< 145°$ for all particles in frame 28455 (preperihelion), therefore focussing plays a minor role, only a broadening of the zero emission velocity case occurs. The spike of frame 29318 is a result of the increasing influence of focussing for old particles and their concentration near $x = 0$. The geometric condition $\psi = 0$ (nodal line) is fulfilled by younger particles in the later observations, as can be seen from Fig. 8.

The spike of frame 29446 was discussed in detail for Figs. 5 and 6. The situation for frame 29760 is similar, but here the x-range of particles with $|\psi - 180°| \leqq 10°$ is larger and shifted

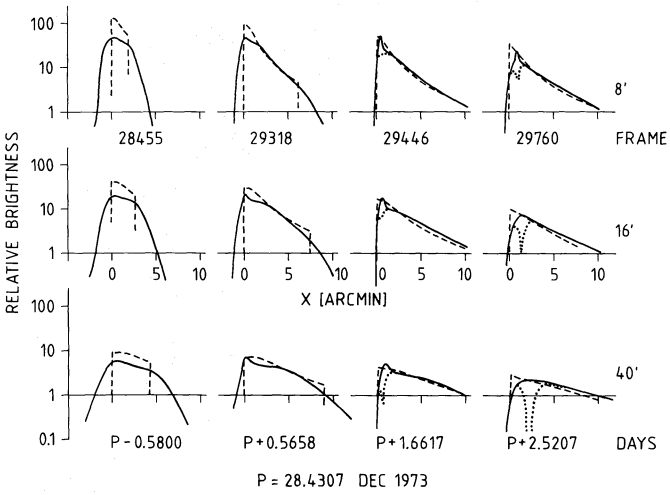

Fig. 7. Calculated relative brightness (logarithmic scale) across the spike of comet Kohoutek for the frames 28455 to 29760 at distances 8′, 16′, and 40′ from the nucleus for the parameter values $s = 1.8$, $z = 2.0$, $\theta = 30°$, and $v_0 = 1\,\mathrm{km\,s^{-1}}$

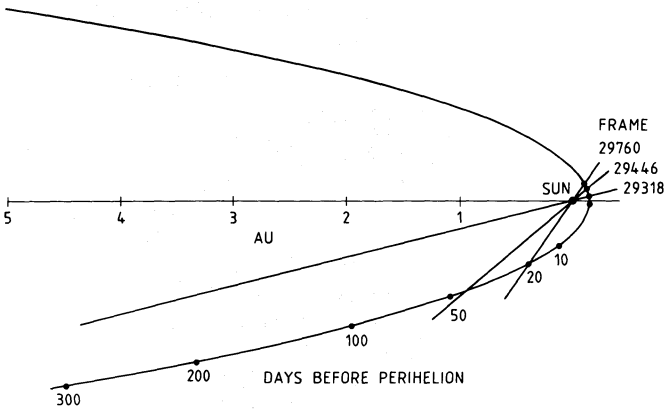

Fig. 8. The orbit of comet Kohoutek (1973 XII) and the nodal lines for the times of frames 29318, 29446, and 2760

to larger northern x-values in the sky plane where younger synchrones are found. In addition, the minimum of the brightness component of particles with $|\psi - 180°| > 10°$ is more pronounced (see dotted lines of Fig. 7). Therefore focussing becomes less important for angular distances greater than about 10′ from the nucleus.

The position angle of the spike directions obtained from the calculated profiles and the corresponding observed spike directions are listed in Table 2. Considering the accuracy of the measured angles and our simplified model, the discrepancies between the observed and calculated spike directions can be accepted. For the frames 28455, 29318, 29446 the spike is well aligned with the sunward directed dashed lines of Fig. 2 that represent the limits for the synchrones for old and large particles. For frame 29760, however, the spike direction has changed northward to the synchrones which belong to younger particles.

Supported by the present calculations, the influence of s and $v_0 \sin\theta_0$ on the profiles of Fig. 7 can be summarized in the following way. With increasing s ($s > 1.8$) the size distribution changes to smaller particles and the anomalous tail extends northward. Consequently the spike, especially for frames 29318

Table 2

Frame	28455	29318	29446	29760
Observed position angle of the spike (taken from Table 1)	256.°0 ± 2°	253.°5 ± 1°	253.°4 ± 1°	260.°1 ± 2°
Position angle of the velocity vector + 180°	254.°5	253.°8	253.°5	253.°4
Angle between the negative velocity vector and the spike direction for the calculated profiles	0.°0	0.°3	1.°1	5.°5
Resulting position angle of the spike direction	254.°5	254.°1	254.°6	258.°9
Difference to the observed directions	1.°5	-0.°6	-1.°2	+1.°2

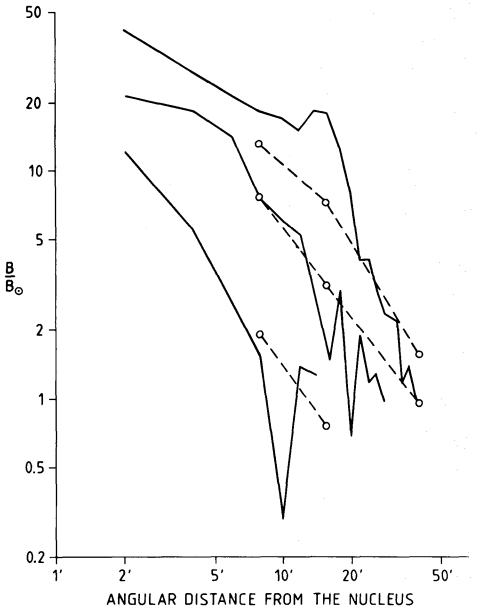

Fig. 9. Measured mean (across 1') brightness curves along the spike for the frames 29318, 29446, and 29760 in units of the mean brightness of the solar disk, $B_0 = 1.98\ 10^5$ stilb. The dashed lines are the corresponding calculated brightness curves

and 29446 becomes less prominent with respect to the fan like part of the tail. On the other hand, if s decreases ($s < 1.8$) the tail seems to be compressed towards the orbit of the comet where $x = 0$. The spike near $x = 0$ becomes stronger, independent of the focussing effect, but the fan like part especially for the frames 28455 and 29318 can no longer be explained. In addition the orientation of the spike does not match the observed spike direction for frame 29760 if $v_0 = 0$.

With increasing θ_0 or v_0 ($v_0 \sin\theta_0 > 0.5\,\mathrm{km\,s^{-1}}$) the profiles broaden and the width of the tail for frame 28455 becomes larger than observed. First the spike remains sharp and appears also for frame 29760 at distances larger than 10′ from the nucleus, later it becomes smoother, too. If θ_0 or v_0 decrease the fully drawn lines of Fig. 7 approach the dashed curves which represent the zero emission velocity case. The tail width calculated for frame 28455 becomes smaller than observed while the distinct spikes change to smoother profiles with only one sharp edge for later dates.

Finally an attempt is made to estimate the total dust production rate by comparison of the observed calibrated brightness with our calculations. As mentioned this is only possible for the spike, the extended flat part of the tail must be removed because we cannot discriminate the stray light from the fan like part in the photographs. Figure 9 shows the mean brightness of the spike within a width of 1′ in units of the mean solar brightness (left hand scale) as a function of the distance from the nucleus for the frames 29318, 29446, and 29760.

The calculated profiles have been adjusted to these curves, they are marked by circles and are connected by dashed lines. The scaling factors for the frames 29760, 29446, and 29318 (with the scattering angles 117°, 129°, 150°) are different; their ratios are 0.55, 0.7, 1.0, respectively. A large white sphere ($a \gg \lambda$) following Lambert's law (Van de Hulst, 1957), irregular particles (Hanner et al., 1981), and the comparison of scattered light to infrared emission of cometary dust particles (Ney, 1982) show an increase of the phase function $\chi(\alpha)$ in the range from 100° to 180°. For $\varrho = 10^3\,\mathrm{kg\,m^{-3}}$, $Q_{\mathrm{pr}} = 1$ and a geometric albedo $A_p = 0.03$ (Divine et al., 1986) we have determined the constant in Eq. (7)

$$N = c\left(\frac{r}{r_0}\right)^{-2} m^{-1.8}\,\frac{dm}{d\beta}\,f(\theta) \tag{7}$$

which is another form of Eq. (4) and found $c = 2.9\ 10^3$; all units are in kg, m, s and $r_0 = 1.496\ 10^{11}$ m. For

$$\dot{M} = \int_{4\pi}\int_{\beta_1}^{\beta_2} N \cdot m\,d\beta\,d\omega \tag{8}$$

it yields

$$\dot{M} = \left(\frac{r}{r_0}\right)^{-2} 1.8\ 10^5\,(m_2^{0.2} - m_1^{0.2}), \tag{9}$$

where m_1, m_2 are the cut offs for small and large particles, respectively. Within our model the largest particles found in the spike correspond to $m_2 \approx 10^{-6}$ kg or $a_2 \approx 0.6\ 10^{-3}$ m. β is limited to $\beta \leqq 1$, therefore $m_1 \approx 10^{-15}$ kg or $a_1 \approx 0.6\ 10^{-6}$ m. Then

$$\dot{M} = \left(\frac{r}{r_0}\right)^{-2} 1.1\ 10^4\,\mathrm{kg\,s^{-1}}. \tag{10}$$

$\dot{M}$ is mainly determined by the cut off for large particles. Sekanina (1974b) found $\dot{M} = 2.5\ 10^4\,\mathrm{kg\,s^{-1}}$ at 1 AU for comet Kohoutek whereas the mass loss rate given by Ney (1982) is about a tenth of our value. However his calculation, based on infrared data, underestimates the contribution from particles larger than a few microns.

Mass loss rates for other comets reduced to 1 AU using the $1/r^2$ law are in the order of several $10^3\,\mathrm{kg\,s^{-1}}$ (Finson and Probstein, 1968; Sekanini and Miller, 1973; Ney, 1982). Sekanina (1974b) pointed out that submillimeter and larger particles do not contribute appreciably to the photometric profiles of regular dust tails. Therefore mass loss rates based on optical observations of normal tails may tend to underestimate the dust production.

6. Conclusion

Generally, the sunward spikes of comet Arend-Roland (1957 III) and comet Kohoutek (1973 XII) are qualitatively interpreted as thin dust layers in the orbital plane of the comet seen edge on from the earth (being near the orbital plane of the comet). Whipple

(1957), Öpik (1958), Gary and O'Dell (1974), and Sekanina (1974b) assumed low emission velocities of large dust particles from the coma to explain the concentration around the orbital plane. Another possibility to concentrate dust in the orbital plane of a comet is derived from the fact that particles ejected from a comet before its perihelion are located again in the cometary orbital plane after $\psi = \pi$ independent of their outflow velocity. Kimura (1979) defined a "neckline" as the locus of particles originally emitted into vertical directions and just recrossing the cometary orbit plane. Kimura (1979), Keller et al. (1983), and Pansecchi et al. (1987) have shown that the focussing of particles around their nodal lines or the so called "necklines" can explain the sharpness of cometary anomalous tails.

Previous attempts to interpret the anomalous tail of comet Kohoutek by zero emission velocity approach are associated with the following problems:

1. The pattern of the synchrones and syndynes changes continuously from frame 28455 to frame 29760 whereas the observed spike remains near the limit for the old synchrones in frames 28455, 29318, and 29446, but turns off northward at about 6° for frame 29760.

2. A major excess of large particles was required to explain the spike (29318, 29446), e.g. $s < 1.8$ but small particles, e.g. $s \geqq 1.8$ were also necessary for the fan like part (28445, 29318). That meant, bimodal size distributions more complicated than $h(m) \propto m^{-s}$ had to be applied.

3. Calculations (Keller et al., 1983) predicted the spike to be present for a longer time, earlier and later than observed.

These problems disappear in the present brightness calculations using reasonable emission velocities ($v_0 = 1\,\mathrm{km\,s^{-1}}$, $\theta_0 = 30°$), a mass distribution $h(m) \propto m^{-1.8}$, and a production rate proportional to $1/r^2$.

As mentioned above v_e from Eq. (2) with $v_0 = 1\,\mathrm{km\,s^{-1}}$ (Sect. 4) and a dust production rate proportional to $1/r^2$ (Sect. 5) are compatible with earlier publications, however, here these distributions are extended to a heliocentric distance range of $0.14 < r < 5$ AU. Particles forming the most prominent focused ($\psi \approx \pi$) anomalous tail of frame 29318 had to be released from the nucleus already at $\gtrsim 5$ AU. Therefore a considerable activity of the new comet far before the onset of water sublimation ($r \lesssim 3$ AU) was required. Comet Kohoutek is a famous example for early activity of incoming new comets. The $1/r^2$ variation of the dust production is certainly an oversimplification. The full cone angle of 60° ($2\theta_0$) can be compared with observations of comet Halley from the spacecraft Giotto (Keller et al., 1987). The present mass distribution exponent $s = 1.8$ is slightly lower than the commonly accepted value of about 2 for particles larger than a few microns (Sekanina, 1980; Hanner, 1980; Divine et al., 1986). Evaporation of dust particles near the sun could possibly depress the intrinsic mass population index (Sekanina, 1974b).

It is concluded that comet Kohoutek produced dust with a more or less "normal" size distribution without a major excess of large particles in contrast to earlier results (Sekanina, 1974b; Keller et al., 1983) and that the effect of focussing is the key to understanding the spike in the comet's anomalous tail at the end of December 1973.

Acknowledgements. The authors thank the White Light Coronagraph team for providing the data. Digitization of the film images was done by Ms. A. Lecinski of HAO, and a special effort to calibrate the off sun images was undertaken by A. Bhomik, A. Stanger, and R. MacQueen of HAO. One of the authors (H. U. Keller) wishes to express his gratitude for the hospitality and support he enjoyed during the observational campaign in December 1973. Many thanks to R. MacQueen and E. Hildner on behalf of the whole team.

References

Bessel, W.: 1836, *Astron. Nachr.* **13**, 185
Bredikhin, F.A.: 1903, Mechanische Untersuchungen über Kometenformen in systematischer Darstellung by R. Jaegermann, St. Petersburg, p. 83
Divine, N., Fechtig, H., Gombosi, T.I., Hanner, M.S., Keller, H.U., Larson, S.M., Mendis, D.A., Newburn, R.L. jr., Reinhard, R., Sekanina, Z., Yeomans, D.K.: 1986, *Space Science Rev.* **43**, 1
Finson, M.L., Probstein, R.F.: 1968, *Astrophys. J.* **154**, 327
Gary, G.A., O'Dell, C.R.: 1974, *Icarus* **23**, 519
Gombosi, T.I., Cravens, T.E., Nagy, A.E.: 1985, *Astrophys. J.* **293**, 328
Hanner, M.S.: 1980, in *Solid Particles in the Solar System*, eds. I. Halliday, B.A. McIntosh, Reidel, Dordrecht, p. 223
Hanner, M.S., Giese, R.H., Weiss, K., Zerull, R.: 1981, *Astron. Astrophys.* **104**, 42
Hellmich, R., 1981, *Astron. Astrophys.* **93**, 341
Keller, H.U., Richter, K., Schmidt, H.U., Hildner, E.: 1983, *Cometary Exploration II*, Proceedings of the International Conference on Cometary Exploration, Budapest, 1982, p. 153
Keller, H.U., Delamere, W.A., Huebner, W.F., Reitsema, H.J., Schmidt, H.U., Whipple, F.L., Wilhelm, K., Curdt, W., Kramm, R., Thomas, N., Arpigny, C., Barbieri, C., Bonnet, R.M., Cazes, S., Coradini, M., Cosmovici, C.B., Hughes, D.W., Jamar, C., Malaise, D., Schmidt, K., Schmidt, W.K.H., Seige, P.: 1987, *Astron. Astrophys.* **187**, 807
Kimura, H.: 1979, in *Dynamics of the Solar System*, ed. R.L. Duncombe, p. 307
MacQueen, R.M., Gosling, I.T., Hildner, E., Munro, R.H., Poland, A.I., Ross, C.L., Keller, H.U., Schmidt, H.-U.: 1974, *Comet Kohoutek Workshop*, Marshall Space Flight Center, p. 19
Ney, E.P.: 1982, in *Comets*, ed. L.L. Wilkening, Tucson, p. 323
Öpik, E.J.: 1958, *Irish Astron. J.* **5**, 37
Pansecchi, L., Fulle, M., Sedmak, G.: 1987, *Astron. Astrophys.* **176**, 358
Probstein, R.F.: 1968, *Problems of Hydrodynamics and Continuum Mechanics*, Soc. for Industrial and Applied Mathematics, Philadelphia, p. 568
Richter, K., Keller, H.U.: 1987, *Astron. Astrophys.* **171**, 317
Sekanina, Z., Miller, F.D.: 1973, *Science* **179**, 565
Sekanina, Z.: 1974a, *Sky Telesc.* **47**, 374
Sekanina, Z.: 1974b, *Icarus* **23**, 502
Sekanina, Z.: 1980, in *Solid Particles in the Solar System*, eds. I. Halliday, B.A. McIntosh, Reidel, Dordrecht, p. 237
Van de Hulst, H.C.: 1957, *Light Scattering by Small Particles*, Wiley, New York
Whipple, F.L.: 1957, *Sky Telesc.* **16**, 426